https://doi.org/10.18321/1101

Oxidation Characteristics of Water Soluble Fractions of Agro-Stalks with Focus on Function of Reactive Inorganics

R. Zhao[1], F. He[1]*, F. Behrendt[1,2], J. Cai[3], A. Dieguez-Alonso[4], Y. Liu[1]

[1]Shandong University of Technology, Zibo, Shandong, 255049, China
[2]Technische Universität Berlin, Berlin, 10623, Germany
[3]Shanghai Jiao Tong University, Shanghai, 200240, China
[4]Otto-von-Guericke-Universität Magdeburg, Magdeburg, 39106, Germany

Article info

Received:
12 March 2021

Received in revised form:
28 April 2021

Accepted:
17 June 2021

Keywords:
Agro-stalks
Water soluble fractions
Oxidation characteristics
Reactive inorganics

Abstract

In order to deepen the understanding of the thermochemical behavior of reactive inorganics, which play an important role in slagging and fouling during combustion of agro-stalks, the oxidation behavior of the water-soluble fraction of corn stover, wheat straw and rice straw was examined using a simultaneous thermogravimetric analyzer. The oxidation characteristics were discussed in combination with elemental analysis of water-soluble fractions. Results showed that reactive inorganics elements account for 30–40% in water-soluble fractions of the three agro-stalks and carbon was oxidized at two separate stages. Four stages were found during oxidation of water-soluble fractions – (1) devolatilisation of organics (100–400 °C); (2) oxidation of char (400–650 °C); (3) oxidation of char with melting of salts or decomposition of carbonate (650–800 °C); (4) vaporization of KCl (800–1000 °C). This work provides a base study for an optimized design of combustion for agro-stalks and pharmaceutical waste.

1. Introduction

The annual consumption of biomass for energetic purposes currently accounts for 8–14% of the world final energy consumption, and its share is increasing rapidly[1]. It is expected that up to 50% of the world's primary energy consumption will be met by biofuels in 2050 [1–3]. The replacement of coal and natural gas by bioenergy can reduce CO_2 emissions[4] and realize the circulation of nutrients [1, 3, 5–7]. However, problems related to ash, including alkali-induced slagging [8–11], corrosion [3, 12], particulate emission [1, 13], and ash nutrients solidification [6, 14] during direct combustion limit the efficient and clean energetic utilization of biomass. High contents of Cl, S, alkali metals (K and Na) in biomass and high temperature in combustion exacerbate these problems [8, 9, 15–18].

Most of the above named reactive inorganic elements in biomass can be extracted by washing with water and these combustion problems are alleviated by pre-treatment of alkali metal leaching [5, 11, 16–22]. The removal ratios of Cl and K from straw with tap-water washing are 87 and 50%, respectively [16]. The removal ratios of K, Cl, S with bath water washing at a constant temperature (25 °C) amount to 80, 90, and 90%, respectively [5]. These removal ratios can be further improved by grinding of the material, fully immersing or bathing using hot water [23], and the alkali of herbaceous biomass are easier to be extracted by water than those of woody biomass [18, 24].

Water-soluble fractions (WSF) of biomass, i.e. the components in water leachate (washed using water) from biomass, contain a large amount of reactive salts (chlorides, sulphates, nitrates, carbonates and alkali metal elements) [2, 5, 16, 24–26] and organics (soluble carbohydrates, organic acids and amino acids/peptides, etc.) [2, 27]. The fractions are characterized by reactive inorganics

*Corresponding author.
E-mail: fanghe916@daad-alumni.de

mixed with large amounts of organics, and it enriches the reactive inorganics in biomass, sharing similarity with pharmaceutical residues [28–30] (which are often incinerated). A deep understanding of the thermochemical conversion characteristics of this type of mixture is important to optimize the combustion process for low-grade solid fuels (low-grade coal, biomass) and biogenic waste (municipal waste, pharmaceutical residue). However, the oxidation characteristics of WSF of biomass have not been investigated.

The thermal conversion of reactive inorganics and their interactions with biomass has been widely investigated. As to the thermal behavior of reactive inorganics, some typical salts (KCl, K_2SO_4, K_2CO_3, $CaCO_3$ and etc.) were rooted from biomass and their mixture was examined using simultaneous thermal analysis (STA). Melting, vaporization, decomposition was observed in some of those compounds. It was found that mass loss is mainly caused by the release of CO_2 from $CaCO_3$ below 850 °C [21, 31]. At temperatures of 850–1150 °C, mass loss is related to vaporization of KCl [31, 32] and release of CO_2 due to reaction of K_2CO_3 with SiO_2 [31]. As to the interaction of reactive inorganics and biomass, thermal behavior of biomass ash with a small number of inorganics, and catalytic properties of reactive inorganics on biomass combustion were investigated with help of X-Ray Fluorescence Spectrometer (XRF), X-ray diffraction (XRD), and STA. Phase transformation of reactive inorganics was found during the heating process. For example, KCl was detected in ash formed at low ash-forming temperature, while K_2SO_4, K_2CO_3 was detected at a high ash-forming temperature [33]. Eutectic melting of KCl and K_2SO_4 occurs around 680 °C [34, 35]. It was also found that potassium salts often work as catalysts in biomass combustion. Compared with water-washed straw, the devolatilization peak temperature and the char-oxidation peak temperature of water-washed straw loaded with different types and concentrations of potassium salt (1–8%) decrease by 25–60 °C and 40–45 °C, respectively [36]. The catalytic effect of potassium monotonously increases with the increase of the concentration of potassium salts loaded [36, 37]. The above mentioned investigations clarify many aspects of the effects of reactive inorganics on organics during combustion. However, due to the small content of reactive inorganics in raw agro-stalks, their effect on the oxidation process is not clearly visible in the combustion of agro-stalks.

In this paper, the effect of reactive inorganics on combustion is investigated via thermal analysis of water-soluble fractions of agro-stalks which enrich reactive inorganic and embody obviously their functions. Corn stover, wheat straw and rice straw were chosen because of their herbal properties and high production in the world.

2. Materials and methods

2.1. Preparation of water-soluble fractions and their microscopic observation

All the agro-stalks are collected from rural areas of Shandong Province, China in 2020. After being air dried in the field, corn stover (CS), wheat straw (WS), rice straw (RS) were crushed into powder with a diameter < 0.5 mm. About 30.0 g of biomass powder and 1500 ml of distilled water were mixed. The mixture was stirred for 5 min in every 1 h at room temperature (26 °C) for a total of 6 h. After that, the mixture was filtered with quantitative filter paper (pore diameter: 30–50 μm, Fushun Civil Administration Filter Paper Factory, China) to obtain a filtrate. Water in the filtrate was removed via evaporation at its boiling point (ca. 103 °C) and followed by drying at 105 °C for 24 h in an electric oven with an air blower (Model 101, Shanghai Keheng Industrial Development Co., LTD, China). These dried filtrates are the WSF of biomass. The WSF account for 6.6±0.2%, 7.0±0.2% and 9.5±0.2% of the mass of CS, WS, RS, respectively in three batches. They were crushed in an agate mortar into powder, passed through 100 mesh sieves, sealed and stored. The experiments were done within a week.

The crystal structure of soluble contents in the filtrates was observed via drying a drop of filtrate on a glass slide by using a microscope (UMT203i R/T Metallurgical Microscope, Chongqing Aopu Optoelectronic Technology Co., LTD, China).

2.2. Elemental and componential analyses of water-soluble fractions

2.2.1. Elemental analysis of raw material

Elemental contents of C, H, N and S in the WSF were measured using an elemental analyzer (Standard deviation: CHNS ≤ 0.1%, Vario EL cube, Elementar, Germany). About 2–3 mg (Weighing Balance Accuracy: 0.001 mg) of WSF sample were used in each of two repeated tests with sulfanilamide as a standard sample and an average value was calculated.

2.2.2. Elemental analysis of reactive inorganics elements

Elemental contents of the reactive inorganic elements were analyzed through X-Ray Fluorescence Spectrometer (XRF, ZSX100e, RIGAKU, Japan). The sample was pressed into a slice with a diameter of 20 mm and a thickness of 3–5 mm. Then it was fully scanned in a vacuum via XRF analyzer. The collected data were processed using a semi-quantitative nonstandard analysis program (SQX) to obtain elemental contents.

It should be noted that signals from XRF analyzer are reliable only for elements with atomic weight more than 23 (eg. K, Cl, Ca, Mg, Na, S), but they are unreliable for C, H, N and O all with atomic-weights below 23 [35]. As a result, only relative ratios between high atomic-weight elements are reliably determined via XRF analysis of WSF of agro-stalks.

2.3. Oxidation behavior of water-soluble fractions

Thermogravimetric (TG: mass-loss rate) and differential scanning calorimetry (DSC: heat effect) during the oxidation of WSF of agro-stalks were recorded simultaneously using a thermogravimetric analyzer (TGA DSC1, Mettler TOLEDO, Switzerland). To avoid corrosion of the instrument by the samples, a pair of crucibles (inner: 50 µl alumina, outer: platinum 70 µl) were used in the experiments. About 3 mg of sample was spread evenly on the bottom of the inner crucible, heated from 100 to 1000 °C at a heating rate of 10 °C/min [5, 16]. Air (21% O_2, 79% N_2, v/v, Shandong Baiyan Chemical Industry Co., LTD, China) with flow rates of 20, 100, 200 ml/min was used as reactive gas and N_2 (>99.9%, Shandong Baiyan Chemical Industry Co., LTD, China) with a flow rate of 20 ml/min was used as protective gas. A blank run was performed before each run of a sample to exclude the influence of the system. Reproducibility was checked by triplicate runs.

2.4. Data processing method

2.4.1. Calculation of elemental content in water-soluble fractions of agro-stalks

Both the content of C, H, N, S from the elemental analyzer (Standard deviation: CHNS ≤ 0.1%) and the relative ratios of heavy elements (M > 23) from XRF analyzer [35] are reliable. The overlap element in the two methods is S. On the basis of this, contents (Y_i, %) of other heavy elements than S are calculated using Eq. 1, and the content (Y_O, %) of oxygen is calculated using Eq. 2 according to mass conservation.

$$Y_i = y_i \cdot Y_S / y_S \tag{1}$$

$$Y_O = 1 - (\sum Y_i + \sum Y_j) \tag{2}$$

where y_i and y_S are the content of heavy element i and that of S from XRF analyzer (%). Y_S is the content of S from the elemental analyzer, (%). Y_j is the content of C, H, N and S from the elemental analyzer (%).

By this procedure, elemental contents of CHNS (Y_j), other heavy elemental (Y_i) and oxygen (Y_O) are determined.

2.4.2 Calculation of mass fraction of KCl

The mass fraction of KCl in WSF of agro-stalk was quantified via two ways. One is based on the above-mentioned elemental contents. Experiments show that the molar content of Cl is much less than K and it is assumed that all Cl exists as KCl. The mass fraction (Y_{KCl}, %) of KCl is calculated using Eq. 3.

$$Y_{KCl} = M_{KCl} \cdot Y_{Cl} / M_{Cl} \tag{3}$$

where Y_{Cl} is the mass fraction of Cl (%), M_{KCl} and M_{Cl} are the relative molecular mass of KCl and Cl. The other is based on the TG data of thermogravimetric analysis. According to our previous study [35], there is a separate peak for the release of KCl in DTG curves of WSF of agro-stalks. The percentage of mass loss in this peak is calculated here as the content of KCl in the sample.

2.4.3. Calculation of mass loss and reaction heat using STA data

There are several stages in the oxidation of WSF of biomass. The mass loss (% of original WSF) of a stage is calculated from TG data as normalized mass difference between its initial and final point.

The reaction heat is calculated using both DSC and TG data. The recorded DSC data (dQ_s/dt) of the sample includes the following parts [38]:

$$dQ_s / dt = m_s c_{p,s} \cdot dT / dt + \dot{m}_s H_s \tag{4}$$

where m_s is the mass of the sample (kg), $\dot{m}_s$ is mass-loss rate of the sample (kg/s), $c_{p,s}$ is the specific heat of the sample (MJ /(kg · K)), H_S is the heat of reaction (MJ/kg).

In a reaction peak, the average heat of reaction can be calculated as:

$$H_s = \int_{t_1}^{t_2} \left(dQ_s/dt - m_s c_{p,s} \cdot dT/dt \right) dt \Big/ \int_{t_1}^{t_2} \dot{m}_s \, dt \quad (5)$$

where t_1 and t_2 are the initial and final time of this peak, (s), $\int_{t_1}^{t_2} \left(dQ_s/dt - m_s c_{p,s} \cdot dT/dt \right) dt$ refers to the integral of heat peak in the DSC curve from t_1 to t_2, refers to the mass loss according to TG data from t_1 to t_2.

3. Results and discussion

3.1. Physical properties of water-soluble fractions

Water soluble fractions are brown with an obvious smell probably due to organic compounds. Crystal structures of the WSF of corn stover (CS), wheat straw (WS), rice straw (RS) are shown in Fig. 1. In the crystal structure of all three samples, parallel short branches growing from long branches appear and the angles between the long and short branches are ca. 80°. Compared with WS, branches in crystals of CS and RS are more regular. One possible reason is the different content of potassium salts.

3.2. Elements and components of water-soluble fractions

Contents of the main elements (>0.1%) of WSF of agro-stalks are shown in Fig. 2. It can be seen that the involved elements and their amounts are similar among the three materials. The shares of inorganics elements (K, Cl, Ca, Mg, Na, S, P, Si, Fe) in WSF of CS, WS and RS are ca. 42, 33 and 37 wt%, respectively. The content of alkali metals (K, Na) in the three WSF is ca. 21 wt%, 19 wt% and 22 wt%, respectively. The most abundant elements are C, O, K, and Cl for all samples. They account for ca. 30, 25, 18 and 10 wt%, respectively. The high molar contents of potassium and chlorine here match with our previous work [35], which showed that only the peak of KCl is present in XRD measurement of all three materials. High molar contents of C, H, O indicate a large amount of organic components like soluble carbohydrates, organic acids etc. in WSF of agro-stalks [27]. According to the organic content of WSF ($m_{organic,WSF}/m_{WSF}$) and its proportion in raw biomass ($m_{WSF}/m_{biomass}$), it could be estimated that ca. 5 wt% of the organic fractions from the raw biomass ($m_{organic,WSF}/m_{biomass}$) was removed by water washing.

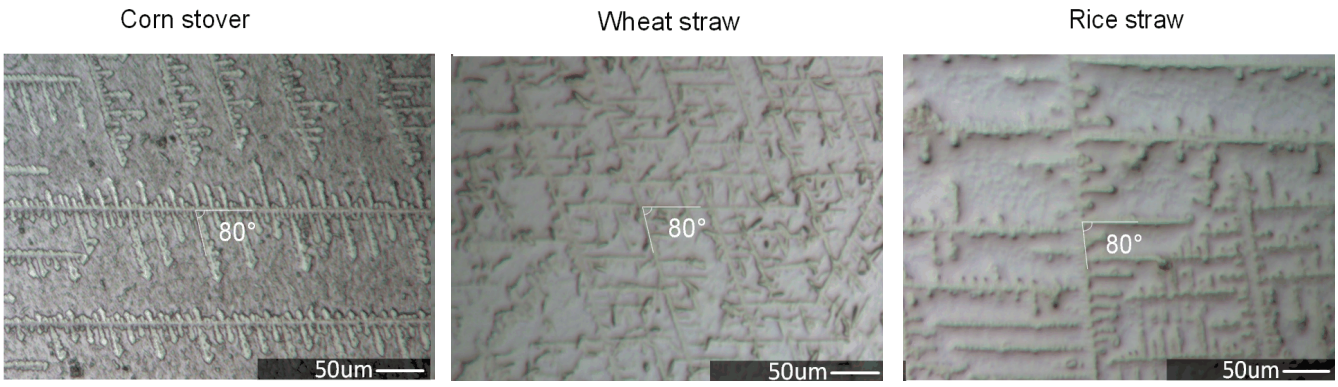

Fig. 1. The crystal structure of water-soluble fractions in the filtrates.

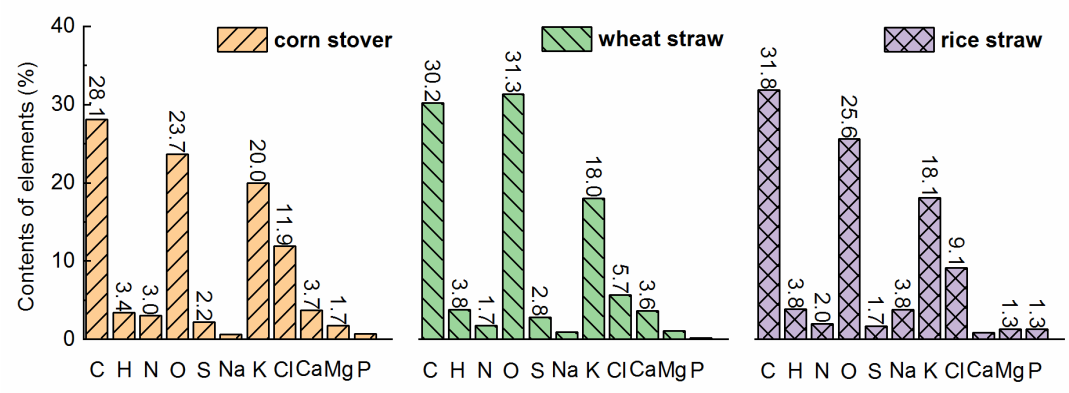

Fig. 2. Elemental contents of water-soluble fractions from agro-stalks.

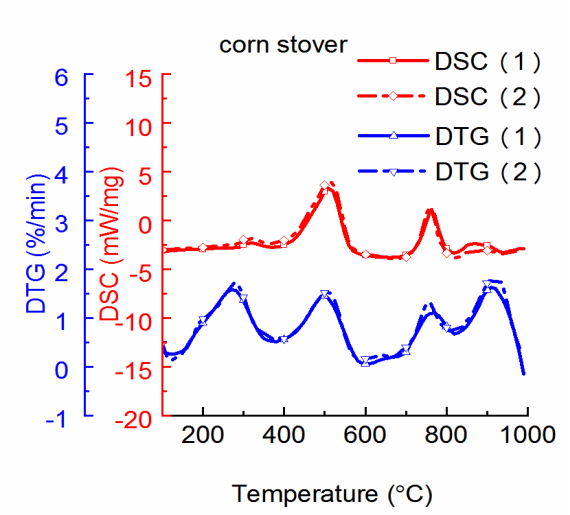

Fig. 3. DSC and DTG curves of water-soluble fractions of corn stover from two repeated experiments.

There are also differences between the three materials. The content of Cl in WSF of WS is lower than in the two others. The content of Na is higher, and that of Ca is lower in WSF of RS than those in the other two materials. These may cause slight differences in the oxidation behavior of the three WSF.

3.3. Oxidation behavior of water-soluble fractions

3.3.1. Reproducibility of oxidation behavior in STA

Experiments on WSF of corn stover heated from 100–1000 °C at a heating rate of 10 °C /min with an air-flow rate of 200 ml/min using STA were repeated twice and TG/DSC results are shown in Fig. 3. Curves of DTG and DSC of the two repetitions overlap well with each other with a maximum relative error <5%.

3.3.2. Four stages of the oxidation process

The TG, DTG and DSC curves of corn stover (CS), wheat straw (WS) and rice straw (RS) at air-flow rates of 20, 100 and 200 ml/min are shown in Fig. 4. In DTG curves with air-flow rates of 100 and 200 ml/min (middle and bottom in Fig. 4), four succeeding mass loss peaks can be observed. For air-flow rates of 20 ml/min (top in Fig. 4), the mass loss peak in DTG curve between 400 and 600 °C is negligible due to the lack of air.

Here, the discussion of four oxidation stages is focused on the cases with air-flow rates of 100 and 200 ml/min due to their obvious oxidation properties. Peak temperatures and temperature ranges of the four stages are shown in Table 1. The temperatures (T_{peaki}) of four succeeding maximum mass-loss rates are the average of $T_{peak\text{-}100}$ from 100 ml/min and $T_{peak\text{-}200}$ from 200 ml/min. The temperature range of each stage is determined as follows. The separation temperature between stage I and II is taken as $(T_{peak1}+T_{peak2})/2$, that between II and III is $(T_{peak2}+T_{peak3})/2$. Between stage III and IV, there is overlap as shown in Fig. 4, and the separation temperature is taken as the turning point.

Within the four stages, stage I and stage II are similar to those observed in the oxidation of biomass. Stage I is similar to devolatilization of biomass [16, 39, 40]. Devolatilization of organic macromolecules such as soluble carbohydrates [27], occurs in this stage. The peak of heat flow in DSC curve is not obvious but the peak of mass loss in DTG curve is clearly visible for all three materials at all three air-flow rates. The mass loss (% of original WSF) varies from 26.7 to 29.9% in ascending order from CS over WS to RS. But the devolatilization temperature of WSF is lower than raw biomass. For wheat stalks and rice stalks, the temperatures of their WSF were 50 and 70 °C lower than that of the raw biomass, respectively [16, 36, 40]. One possible reason is the catalytic effect of the potassium salts, which is abundant in WSF on devolatilization [10, 36, 41, 42]. Another reason is that the organic fractions (sugars, amino acids and peptides) in WSF are easier to pyrolyze than cellulose and hemicellulose in raw biomass.

Table 1
Average peak temperature and temperature range of four stages of oxidation with air-flow rates of 100 and 200 ml/min

Sample	Temperature range (± 5 °C)				Peak temperature: T_{peak} (± 5 °C)			
	I	II	III	IV	I	II	III	IV
CS	100-380	380-630	630-830	830-1000	265	500	755	917
WS	100-400	400-655	655-810	810-1000	250	550	760	895
RS	100-380	380-650	650-810	810-1000	235	530	775	880

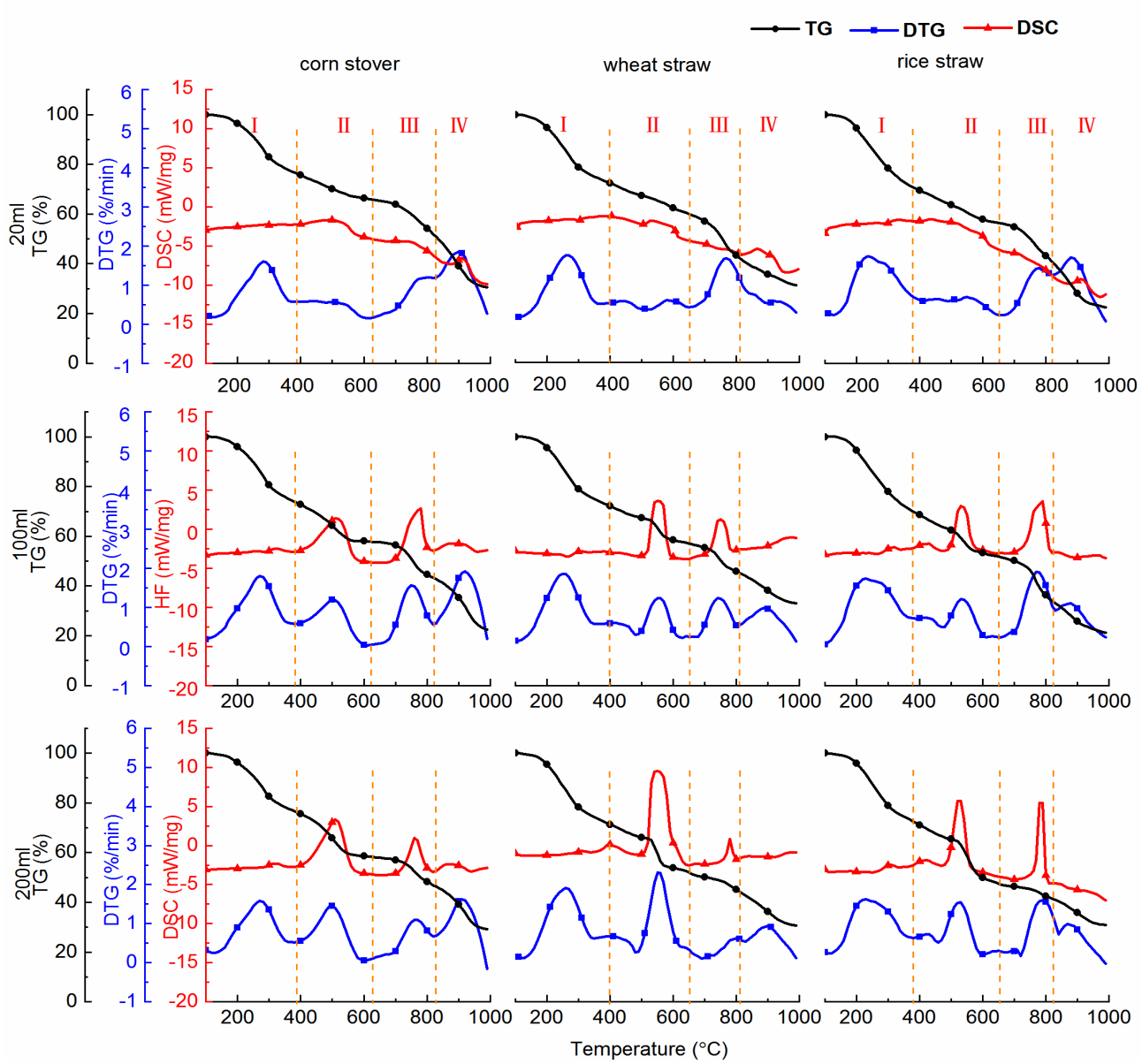

Fig. 4. Result of STA experiments: Mass loss (TG), mass-loss rate (DTG), heat effect (DSC) curves of samples starting from 100 to 1000 °C at the heating rate of 10 K/min at air-flow rate of 20 ml/min (Top), 100 ml/min (Middle) and 200 ml/min (Bottom).

Stage II is similar to char oxidation in biomass combustion [16, 39, 40]. There is an obvious exothermic peak in the DSC curve with a corresponding mass loss peak in the DTG curve. Mass loss (% of original WSF) and reaction heat at stage II are shown in Table 2. The mass loss increases slightly with the increase of air-flow rate from 100 to 200 ml/min. The average reaction heat is 11–25 MJ/kg, between the reaction heat of carbon to CO (9.2 MJ/kg) and to CO_2 (32.8 MJ/kg). Compared with raw biomass, the peak temperature of char oxidation of WSF is ca 100 °C higher than that of raw biomass [16, 36, 40]. A possible reason is the larger inorganic fractions in char from WSF than that from biomass [42].

Stage III and stage IV are quite complex and are discussed in Sections 3.3.3 and 3.3.4.

3.3.3. Stage III: Oxidation of char with the melting of salts and decomposition of carbonate

In stage III with air-flow rates of 100 and 200 ml/min, there is an obvious mass loss peak in DTG curve corresponding with an obvious exothermic peak in DSC curve, similar to that in stage II. Most of the calculated reaction heat in stage III is around 12 MJ/kg. For all elements shown in Fig. 2, only carbon oxidation can have such a high heat effect and mass-loss rate.

Table 2
Mass loss (% of original WSF) and average reaction heat at peaks in stage II and III

Peaks in stage	Air-flow rate (ml/min)	Mass loss (%)			Average reaction heat (MJ/kg)		
		CS	WS	RS	CS	WS	RS
II	100	16.4	10.6	10.7	17.1	22.0	18.1
	200	17.9	14.5	16.6	18.3	25.1	11.6
III	100	14.2	11.0	16.1	12.7	10.3	12.4
	200	10.8	6.2	5.0	13.8	6.2	11.9

In order to test if there is carbon oxidation in stage III, intermediate samples from the oxidation process of 100–650 °C instead than of the previous 100–1000 °C with an air-flow rate of 100 ml/min were prepared and the carbon contents in them were quantified using the element analyzer. Results show that the carbon content ($C_{650} = m_{C650}/m_{650}$) in intermediate residues from WSF of CS, WS and RS are 29.4, 17.8, and 24.7 wt%, respectively. From TG data, the mass ratio ($R_{650} = m_{650}/m_{WSF}$) of the intermediate sample to the original WSF for CS, WS, and RS, are 57.8, 57.1, and 51.9 wt%, respectively. Then, carbon (C_{III}, % of original WSF, m_{C650}/m_{WSF}) in the intermediate sample is calculated as $C_{650} \cdot R_{650}$. They are 17.0, 10.1, and 12.8%, respectively.

Comparison of carbon (C_{III}, % of original WSF) in an intermediate sample with mass loss (TG_{III}, % of original WSF) of stage III with an air-flow rate of 100 ml/min is shown in Fig. 5. It shows that the two corresponding values are close to each other with relative differences of 12.6, 15.1, and 19.5% ($(C_{III}\text{-}TG_{III})/TG_{III} \cdot 100\%$) for the three materials, respectively. Observation also shows that the above-mentioned intermediate sample is black while the final residue of the oxidation process is white. All of these indicate that in stage III, part of the carbon in WSF is oxidized.

Table 2 shows that heat release of unit mass loss in stage III is much lower than the average reaction heat in stage II. There are two possible reasons for this. The first one is the increase of CO/CO_2 ratio with increasing temperature as described by $CO/CO_2 = A \cdot \exp(-E/RT)$ [19, 43], which reduces the reaction heat of char oxidation.

The second possible reason is that some endothermic processes occur simultaneously at this stage. The slow endothermic effect in DSC curves at an air-flow rate of 20 ml/min also indicates this. Salt melting and decomposition of $CaCO_3$ are possible processes. At low temperature, the carbon is isolated from oxygen in gas because of the covering and mixing of salts. When the temperature rises, the salts begin to melt, (eutectic melting of KCl and K_2SO_4 occurs at 680 °C during combustion of herbaceous biomass[35]), and $CaCO_3$ begins to decompose (starts from 550 °C and ends at ca. 800 °C [21, 31, 33]). The carbon is exposed to the gas phase (including oxygen) and oxidation occurs again.

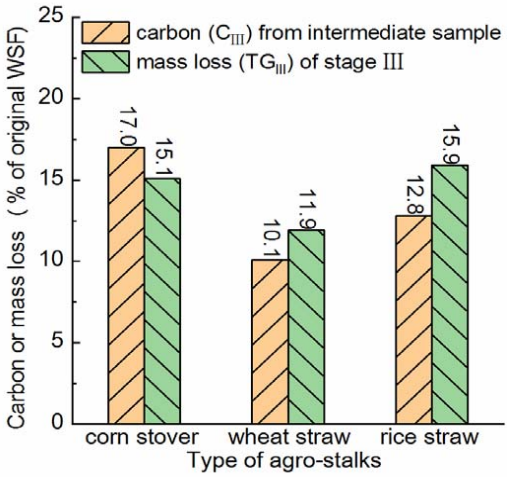

Fig. 5. Comparison of carbon (C_{III}, % of original WSF) in an intermediate sample with mass loss (TG_{III}, % of original WSF) of stage III at an air-flow rate of 100 ml/min.

As a summary, carbon oxidation in WSF occurs in two stages. Below 650 °C, part of the carbon is oxidized. Between 650–800 °C, the residual covered carbon is oxidized due to the melting of salts or decomposition of carbonates.

3.3.4. Stage IV: Vaporization of KCl

In stage IV for all three air-flow rates, there is an obvious mass loss peak in DTG curves but no obvious heat effect peak in DSC curves. In our previous study [32] and other researchers' work [21, 31] on the release of KCl in biomass combustion, shows that vaporization at 800–1000 °C dominates the release of KCl. This indicates that the mass loss peak in stage IV is the vaporization of KCl in this experiment. Compared with reaction heat of char oxidation, the heat effect of KCl vaporization is

negligible, which is the reason for obvious mass loss and negligible heat effect in curves from STA.

Mass loss (% of original WSF) calculated according to TG data in stage IV with different air-flow rates are shown in Fig. 6. For CS, WS and RS, they are 19.2±2.1%, 12.3±1.3%, and 14.3±3.9%, respectively. It is seen that the mass loss deviation among different materials is bigger than that among different air-flow rates.

Calculated contents (% of original WSF) of KCl in three samples according to contents of Cl as mentioned in part 2.4.2 are also shown in Fig. 6. The shares of KCl in three materials are ca. 25, 12, and 19%, respectively. It can be seen that these contents of KCl are close to the mass loss in stage IV. The relative differences between contents of KCl and mass loss at stage IV based on the content of KCl ranges from 1.5 to 36.4%. Besides of the error of measurement, the possible reasons of this difference are the decomposition of K_2CO_3 [21], the transformation of KCl to K_2SO_4 with release of Cl_2 [44] and the unclear separation temperature between stage III and IV.

All the above results show that most KCl in WSF of agro-stalks is vaporized during its slow oxidation in STA. In order to facilitate the oxidation of carbon and reduce the vaporization of KCl during the oxidation of organics with high content of reactive inorganics, the temperature should be about 810 °C.

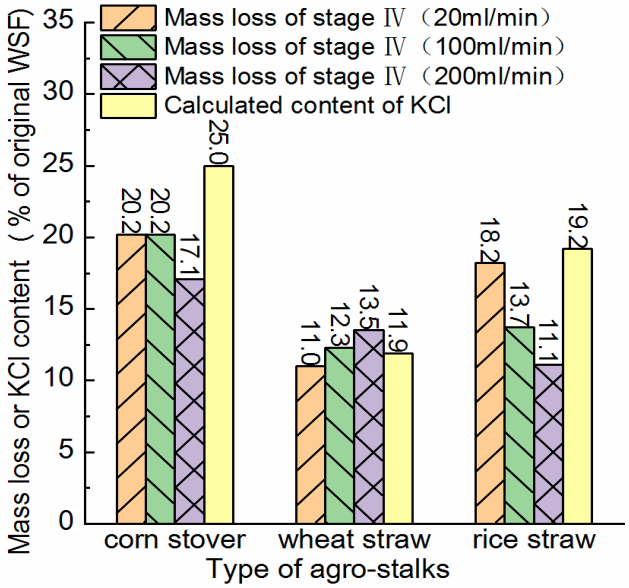

Fig. 6. Comparison of the calculated KCl content (% of original WSF) based on content of Cl in WSF with mass loss (% of original WSF) of WSF at stage IV (from 810–1000 °C) in STA at different air-flow rates (20, 100, 200 ml/min).

5. Conclusions

The composition and oxidation behavior of water-soluble fractions (WSF) from CS, WS and RS were examined. Results show that the components and oxidation characteristics of the three materials are similar as following:

1) WSF from agro-stalks are a mixture of ca. 35 wt% reactive inorganics (K, Cl, Ca, Mg, Na, S) and 65 wt% organics (soluble carbohydrates and organic acids etc.).

2) There are four stages in the oxidation of WSF. Carbon is oxidized in two stages due to the interaction of inorganics with organics.

3) Most KCl vaporize at 800–1000 °C during slow oxidation of WSF in STA.

The result can be used as a reference in the optimization design of combustion for agro-stalks and pharmaceutical waste.

Acknowledgments

The authors gratefully acknowledge financial support from the National Natural Science Foundation of China (grant no. 51676115) and Sino-German Center for Research Promotion (grant no. M-0183).

References

[1]. A. Williams, J.M. Jones, L. Ma, M. Pourkashanian, *Prog. Energy Combust. Sci.* 38 (2012) 113–137. DOI: 10.1016/j.pecs.2011.10.001

[2]. S.V. Vassilev, C.G. Vassileva, *Energy Fuels* 33 (2019) 2763–2777. DOI: 10.1021/acs.energyfuels.9b00081

[3]. Y. Niu, H. Tan, S. Hui, *Prog. Energy Combust. Sci.* 52 (2016) 1–61. DOI: 10.1016/j.pecs.2015.09.003

[4]. Y.-J. Lee, J.-W. Choi, J.-H. Park, H. Namkung, G.-S. Song, S.-J. Park, D.-W. Lee, J.-G. Kim, C.-H. Jeon, Y.-C. Choi, *ACS Sustainable Chem. Eng.* 6 (2018) 13056–13065. DOI: 10.1021/acssuschemeng.8b02588

[5]. L. Deng, T. Zhang, D. Che, *Fuel Process. Technol.* 106 (2013) 712–720. DOI: 10.1016/j.fuproc.2012.10.006

[6]. Z. Zhang, F. He, Y. Zhang, R. Yu, Y. Li, Z. Zheng, Z. Gao, *J. Clean. Prod.* 170 (2018) 379–387. DOI: 10.1016/j.jclepro.2017.09.150

[7]. A. Babin, C. Vaneeckhaute, M.C. Iliuta, *Biomass Bioenerg.* 146 (2021) 105968. DOI: 10.1016/j.biombioe.2021.105968

[8]. Q.H. Li, Y.G. Zhang, A.H. Meng, L. Li, G.X. Li, *Fuel Process. Technol.* 107 (2013) 107–112. DOI: 10.1016/j.fuproc.2012.08.012

[9]. A. Rebbling, I.-L. Näzelius, M. Schwabl, S. Feldmeier, C. Schön, J. Dahl, W. Haslinger, D. Boström, M. Öhman, C. Boman, *Biomass Bioenerg.* 137 (2020) 105968. DOI: 10.1016/j.biombioe.2020.105557
[10]. Q. Liu, S.C. Chmely, N. Abdoulmoumine, *Energ. Fuel.* 31 (2017) 3525–3536. DOI: 10.1021/acs.energyfuels.7b00258
[11]. M. Zevenhoven, P. Yrjas, B.-J. Skrifvars, M. Hupa, *Energ. Fuel.* 26 (2012) 6366–6386. DOI: 10.1021/ef300621j
[12]. C. Yin, L.A. Rosendahl, S.K. Kær, *Prog. Energy Combust. Sci.* 34 (2008) 725–754. DOI: 10.1016/j.pecs.2008.05.002
[13]. O. Sippula, H. Lamberg, J. Leskinen, J. Tissari, J. Jokiniemi, *Fuel* 202 (2017) 144–153. DOI: 10.1016/j.fuel.2017.04.009
[14]. Y. Zhang, F. He, Z. Gao, Y. You, P. Sun, *Fuel* 162 (2015) 251–257. DOI: 10.1016/j.fuel.2015.09.025
[15]. P. Brassard, J.H. Palacios, S. Godbout, D. Bussières, R. Lagacé, J.-P. Larouche, F. Pelletier, *Bioresour. Technol.* 155 (2014) 300–306. DOI: 10.1016/j.biortech.2013.12.027
[16]. N. Said, T. Bishara, A. Garcia-Maraver, M. Zamorano, *Waste Manage.* 33 (2013) 2250–2256. DOI: 10.1016/j.wasman.2013.07.019
[17]. P. Thy, C. Yu, B.M. Jenkins, C.E. Lesher, *Energ. Fuel.* 27 (2013) 3969–3987. DOI: 10.1021/ef400660u
[18]. A. Saddawi, J.M. Jones, A. Williams, C. Le Coeur, *Energ. Fuel.* 26 (2012) 6466–6474. DOI: 10.1021/ef2016649
[19]. D. Vamvuka, D. Zografos, G. Alevizos, *Bioresour. Technol.* 99 (2008) 3534–3544. DOI: 10.1016/j.biortech.2007.07.049
[20]. H. Namkung, Y.-J. Lee, J.-H. Park, G.-S. Song, J.W. Choi, J.-G. Kim, S.-J. Park, J.C. Park, H.-T. Kim, Y.-C. Choi, *Energy* 187 (2019) 115950 DOI: 10.1016/j.energy.2019.115950
[21]. A. Mlonka-Mędrala, A. Magdziarz, M. Gajek, K. Nowińska, W. Nowak, *Fuel* 261 (2020) 116421. DOI: 10.1016/j.fuel.2019.116421
[22]. D.S. Chandler, F.L.P. Resende, *Biomass Bioenerg.* 113 (2018) 65–74. DOI: 10.1016/j.biombioe.2018.03.008
[23]. P. Abelha, C. Mourão Vilela, P. Nanou, M. Carbo, A. Janssen, S. Leiser, *Fuel* 253 (2019) 1018–1033. DOI: 10.1016/j.fuel.2019.05.050
[24]. M.A. Carrillo, S.A. Staggenborg, J.A. Pineda, *Fuel* 116 (2014) 427–431. DOI: 10.1016/j.fuel.2013.08.028
[25]. Y. Niu, Y. Lv, X. Zhang, D. Wang, P. Li, S. Hui, *Appl. Therm. Eng.* 154 (2019) 485–492. DOI: 10.1016/j.applthermaleng.2019.03.124
[26]. S.V. Vassilev, D. Baxter, L.K. Andersen, C.G. Vassileva, T.J. Morgan, *Fuel* 94 (2012) 1–33. DOI: 10.1016/j.fuel.2011.09.030
[27]. Z. He, J. Mao, C.W. Honeycutt, T. Ohno, J.F. Hunt, B.J. Cade-Menun, *Biol. Fertil. Soils* 45 (2009) 609–616. DOI: 10.1007/s00374-009-0369-8
[28]. P.C. Hsu, K.G. Foster, T.D. Ford, P.H. Wallman, B.E. Watkins, C.O. Pruneda, M.G. Adamson, *Waste Manage.* 20 (2000) 363–368. DOI: 10.1016/S0956-053X(99)00338-4
[29]. C. Lin, Y. Chi, Y. Jin, H. Song, *Procedia Environ. Sci.* 31 (2016) 335–344. DOI: 10.1016/j.proenv.2016.02.045
[30]. Z. Yao, J. Li, X. Zhao, *Chemosphere* 84 (2011) 1167–1174. DOI: 10.1016/j.chemosphere.2011.05.061
[31]. S. Arvelakis, P.A. Jensen, K. Dam-Johansen, *Energ. Fuel.* 18 (2004) 1066–1076. DOI: 10.1021/ef034065+
[32]. X. Li, F. He, X. Su, F. Behrendt, Z. Gao, H. Wang, *Fuel* 257 (2019) 116021. DOI: 10.1016/j.fuel.2019.116021
[33]. S. Du, H. Yang, K. Qian, X. Wang, H. Chen, *Fuel* 117 (2014) 1281–1287. DOI: 10.1016/j.fuel.2013.07.085
[34]. X. Li, F. He, F. Behrendt, Z. Gao, J. Shi, C. Li, *Fuel* 289 (2021) 119754. DOI: 10.1016/j.fuel.2020.119754
[35]. F. He, X. Li, F. Behrendt, T. Schliermann, J. Shi, Y. Liu, *Fuel Process. Technol.* 198 (2020) 106231. DOI: 10.1016/j.fuproc.2019.106231
[36]. S. Deng, X. Wang, J. Zhang, Z. Liu, H. Mikulčić, M. Vujanović, H. Tan, N. Duić, *J. Environ. Manage.* 218 (2018) 50–58. DOI: 10.1016/j.jenvman.2018.04.057
[37]. A. Saddawi, J.M. Jones, A. Williams, *Fuel Process. Technol.* 104 (2012) 189–197. DOI: 10.1016/j.fuproc.2012.05.014
[38]. F. He, W. Yi, X. Bai, *Energy Convers. Manage.* 47 (2006) 2461–2469. DOI: 10.1016/j.enconman.2005.11.011
[39]. M.S. Reza, S.N. Islam, S. Afroze, M.S.A. Bakar, J. Taweekun, A.K. Azad, *Data in Brief* 30 (2020) 105536. DOI: 10.1016/j.dib.2020.105536
[40]. F. Sher, S.Z. Iqbal, H. Liu, M. Imran, C.E. Snape, *Energy Convers. Manage.* 203 (2020) 112266. DOI: 10.1016/j.enconman.2019.112266
[41]. J.M. Jones, L.I. Darvell, T.G. Bridgeman, M. Pourkashanian, A. Williams, *Proc. Combust. Inst.* 31 (2007) 1955–1963. DOI: 10.1016/j.proci.2006.07.093
[42]. M. Xu, C. Sheng, *Energ. Fuel.* 26 (2011) 209–218. DOI: 10.1021/ef2011657
[43]. X. Tian, Y. Wang, Z. Zeng, L. Dai, Y. Peng, L. Jiang, X. Yang, L. Yue, Y. Liu, R. Ruan, *Bioresour Technol.* 320 (2021) 124415. DOI: 10.1016/j.biortech.2020.124415
[44]. S.V. Vassilev, D. Baxter, L.K. Andersen, C.G. Vassileva, *Fuel* 105 (2013) 40–76. DOI: 10.1016/j.fuel.2012.09.041